Automatic mode tracing of dispersion relations for guided waves in elastic waveguides via physics-driven affinity propagation (AP) clustering

Xudong Yu[a,*], Bohan Liu[a], Hai Shen[a], Peng Zuo[b], Zheng Fan[c,*]

[a]*School of Astronautics, Beihang University, Beijing, 100191, China*
[b]*Advanced Remanufacturing and Technology Centre, 3 CleanTech Loop, #01/01, CleanTech Two, Singapore 637143*
[c]*School of Mechanical and Aerospace Engineering, Nanyang Technological University, 50 Nanyang Avenue, Singapore 639798*

Abstract

Guided ultrasonic waves are valuable screening tools for elongated engineering structures due to their ability to propagate over long distances and flexibility in selecting mode-frequency combinations. Computing dispersion relations and tracing dispersion curves of guided waves are essential for their NDT/SHM applications. Dealing with complex waveguide problems often necessitate numerical approaches to obtain all the wavenumbers at discrete frequencies. Manual routines are usually adopted to trace different guided wave modes, as they possess distinct set of propagation characteristics, such as polarization, field distribution and so forth. However, challenges arise in intricate scenarios like mode coupling, veering, and splitting, particularly in structures with irregular geometries, anisotropic material properties, or when subjected to perturbations. To address this, we propose an innovative physics-driven mode-tracing technique that features the Affinity Propagation (AP) clustering. Upon solving the associated eigenvalue waveguide problem, the distance measurement between all frequency-discrete eigen-solutions is performed based on the weighted cosine distance. A similarity matrix is thus constructed via the similarity propagation. High-quality set of exemplars and corresponding clusters can be iteratively obtained using the optimized AP clustering algorithm, i.e., accurately tracing guided wave modes. This paper presents the principals of the proposed technique, and then validates and illustrates its use through typical numerical examples. Its robustness is also discussed by varying crucial parameters, including neighborhood size and frequency step. The series of accurate clustering results have manifested the proposed mode-tracing technique as an invaluable tool for determining dispersion relations in complex waveguides, potentially advancing quantitative NDE and SHM.

Keywords: Guided waves, Automated mode-tracing tool, Dispersion curves, Affinity Propagation clustering, Complex waveguide problems

1. Introduction

Guided ultrasonic waves have gained considerable research interest in non-destructive evaluation (NDE) [1, 2, 3, 4], structural health monitoring (SHM) [5, 6, 7, 8], and material characterization [9, 10, 11, 12] over recent decades. This fascination arises from their capability to access elongated structures from a distance, identify discontinuities along the propagation path, and encapsulate insights into the material constitution and stress state of the test elastic waveguides. The utmost significance within the associated

*Corresponding author
Email addresses: `yxudong@buaa.edu.cn` (Xudong Yu), `zfan@ntu.edu.sg` (Zheng Fan)

NDE/SHM techniques lies in the accurate determination of the guided wave modes' dispersion relations, including phase velocity, energy velocity, and attenuation ratio across frequencies [13, 14, 15, 16, 17, 18].

Methods to compute dispersion relations of elastodynamic guided waves encompass analytics and numerics. Analytical methods that involve solving dispersion equations or utilizing matrix techniques [19] are effective in predicting dispersion curves for waveguides of regular geometries, such as flat plates and cylindrical structures. However, for waveguides with irregular-shaped cross-sections, such as rails and bars, their dispersion equations become transcendent, necessitating numerical solutions. Numerical methods, including the semi-analytical finite element (SAFE) method [20, 21, 22], scaled boundary finite element method (SBFEM) [23], wave finite element method (WFEM) [24, 25] and Floquet finite element method (Floquet FEM) [26] are employed to solve the eigenvalue problem in the frequency domain. The resulting frequency-discrete eigen-solutions must then be traced and connected to continuous modes. Such process is usually implemented via manual routines, where mode shapes between eigen-modes at adjacent frequencies are compared. However, this approach sometimes fails when dealing with waveguide problems characterized by intricate material/structural complexity and boundary conditions.

Such failures are attributed to complex and even unpredictable dispersion behaviors of guided wave modes that can exist within a waveguide. Mode coupling, splitting, and veering often occur in structures with irregular geometries or anisotropic material properties, and in waveguides subjected to perturbations or asymmetries [27, 28]. These complex guided wave phenomena, appeared in their dispersion curves, cause uncertainty in mode tracing and hence result in tracing errors. Moreover, in order to accurately capture and accommodate the intricacies of dispersion curves, a significantly refined frequency discretization step is essential for solving the eigenvalue problem, which in turn incurs substantial computational expenses. As a result, researchers are seeking alternative mode-tracing methods to comprehensively and accurately track the dispersion curves, in an efficient manner.

Such attempts encompass the utilization of extrapolation, optimization techniques and the Modal Assurance Criterion (MAC) [29] based method. The extrapolation methods commence from an initial eigen-solution, gradually advancing through small frequency increments to converge upon subsequent eigen-solutions using polynomial expansion. These were initially utilized for regular waveguides and have hence been well implemented in software "*Disperse*", developed by the NDE group at Imperial College London [30]. It has been well-known for its capability to find roots and trace dispersion relations by three orders of Taylor expansion to handle the plate and cylindrical structures with uniformly distributed immersed/embedded boundary conditions. Furthermore, higher order derivatives of eigenvalue problems can be computed analytically and used to extrapolate extended sections of guided waves' dispersion curves by means of high order of Taylor and Padé approximations [31]. Critical frequency regions, i.e., in proximity of mode veering and cutoffs, can be well traced in their dispersion curves. More recently, a so-called kriging metamodeling approach in combination with WFEM, has been proposed to predict the dispersion curves in the beam and thin walled structures [32]. The associated mode tracing was performed via solving an optimization problem regarding the kriging predictor of wavenumber. The aforementioned methods rely on tracing through eigen-solutions, while alternative approaches explore mode tracing via eigenvectors. For instance, the MAC-based technique aims to quantify modal similarity using eigenvectors, and a higher similarity score indicates a greater likelihood of two eigen-solutions belonging to the same mode. The key drawback of the MAC is its inability to provide an absolute measure of similarity between eigenvectors due to the [0,1] rank limitation [33], hindering precise assessment of guided wave mode correspondence. These techniques have proven been effective in tracing guided wave modes' dispersion curves during the concurrent computation of eigen-solutions. However, the sophisticated processes as well as constraints inherent to custom-developed codes have unavoidably restricted their widespread adoption in mode-tracing for complex waveguide problems.

In this study, we propose an automated mode-tracing capability that will be employed once eigen-solutions to a specific eigenvalue problem are obtained. It can provide versatility in tracing the dispersion relations of guided wave modes, independent of the computation procedures, thereby accommodating complicated propagative behaviors across a broad spectrum of both frequencies and eigen-modes. In the context of SAFE calculations, the cosine distances between all the frequency-discrete eigen-solutions are evaluated from the corresponding eigenvectors by weighting their physical characteristics, that encompass the fields of displacement, power flow density, and angular momentum. A similarity matrix is then constructed based on the weighted cosine distances and similarity propagation. An optimized Affinity Propagation (AP) serves as an automatic tool to process the similarity matrix among all the eigen-solutions, iteratively obtaining a high-quality set of exemplars and corresponding clusters, representing different guided wave modes. This process can be carried out without prescribing the number of clusters or other manual interventions in the clustering. We further validate the effectiveness of this tool through typical numerical examples, encompassing the mode-tracing of guided waves in anisotropic viscoelastic media, close/open waveguides with arbitrary cross section, and arbitrarily prestressed waveguides.

To formulate and discuss this approach, the paper is organized as follows. The principle of the mode-tracing tool, characterized by physics-driven feature extraction and AP clustering, is first demonstrated. Following that, several typical numerical evaluations are given to illustrate the utilization of this approach for tracing complex dispersive relations. Finally, we discuss its robustness by varying two crucial parameters, including the neighborhood size and frequency discretization size, and recommendations of using the mode-tracing tool are given as well.

2. Methodology

This section demonstrates an overview of the proposed automatic mode-tracing technique that utilizes Affinity Propagation, in the context of SAFE calculation. First of all, the governing equations of guided waves in elastic waveguides are briefed and the derivation of main physical characteristics are given. Next, the techniques for weighted cosine distance measurement and construction of similarity matrix are proposed. Lastly, the process of mode tracing via AP clustering is described.

2.1. Governing equations

Considering an elongated waveguide with arbitrary cross-section (in $x_1 - x_2$ plane), the waves are assumed to propagate harmonically along the x_3 direction with wavenumber k at the angular frequency $w = 2\pi f$, as schematically shown in Fig. 1. The particle displacement $\boldsymbol{u}$ of the propagating wave field can be given by

$$u_r(x_1, x_2, x_3, t) = U_r(x_1, x_2)e^{I(kx_3 - wt)}, I = \sqrt{(-1)}, \tag{1}$$

where t is the time variable; and the subscript $r = 1, 2, 3$ denotes the coordinate index. The equation of dynamic equilibrium for general anisotropic media can be written in the form of an eigenvalue problem [21]. Let C_{sprq} be the stiffness moduli with real or complex values for elastic or viscoelastic materials respectively [34], and the equations read

$$C_{sprq}\frac{\partial^2 U_r}{\partial x_p \partial x_q} + I(C_{s3rp} + C_{spr3})\frac{\partial(kU_r)}{\partial x_p} - kC_{s3r3}(kU_r) + \rho\omega^2\partial_{sr}U_r = 0, \tag{2}$$

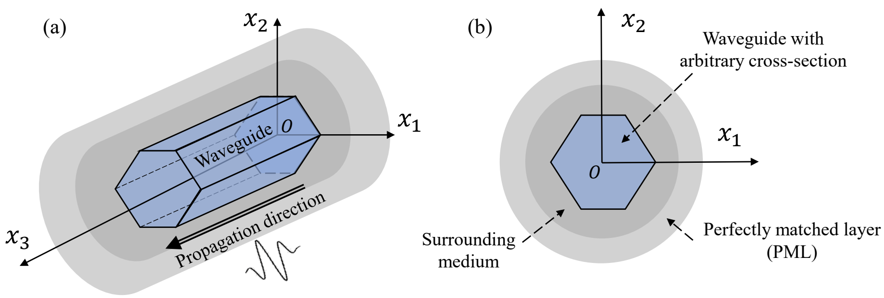

Figure 1: Schematics of (a) a three-dimensional waveguides embedded in infinite medium; the direction of guided wave propagation indicated; (b) a typical two-dimensional SAFE model for a solid waveguide of arbitrary cross-section embedded in the surrounding medium, combined with the perfectly matched layer (PML).

with summation over the indices $r = 1, 2, 3$ and $p, q = 1, 2$; ρ is the mass density. The eigenvalue problem can then be solved for the eigen-wavenumber k and associated eigenvector, using a commercial finite element (FE) package [35].

Through the SAFE calculations, the particle velocity can be derived from particle displacement as $\boldsymbol{v} = d\boldsymbol{u}/dt$; and the stress and strain fields, denoting as $\boldsymbol{\varepsilon}$ and $\boldsymbol{\sigma}$, can be calculated as $\varepsilon_{ij} = \frac{1}{2}[\nabla u_{i,j} + \nabla u_{j,i}]$ and $\sigma_{ij} = C_{ijkl}\varepsilon_{kl}$, respectively. The complex Poynting vector $\boldsymbol{P}$ [36], representing the power flow density of the guided waves, can be calculated from the particle velocity and stress fields based on the following equation:

$$\boldsymbol{P} = -\frac{\boldsymbol{v}^* \cdot \sigma}{2}, \tag{3}$$

where $\boldsymbol{v}^*$ denotes the conjugate of particle velocity vector. Its quantity P_1, P_2 and P_3, of the mode can be obtained at each nodal position over the cross section of the waveguide at all three orthogonal directions, thus achieving the cross-sectional distribution of power flow density of the guided mode at particular frequencies.

Noteworthily, in irregular-shaped waveguides or those with asymmetry, the guided waves' particle displacement is spatially dependent. In order to fully capture the features of their wave structures, an angular momentum associated with the particle velocity was used to describe the rotational motion of particles around the waveguide axis, as the guided wave passes through. Herein, the field quantity of angular momentum $\boldsymbol{L}$ is merged from nodal coordinates and particle velocity across the cross section of the waveguide, which can be given as

$$\boldsymbol{L} = \begin{vmatrix} \vec{i} & \vec{j} & \vec{k} \\ r_1 & r_2 & r_3 \\ v_1 & v_2 & v_3 \end{vmatrix}, \tag{4}$$

where $\vec{i}, \vec{j}, \vec{k}$ represent the unit vectors in x_1, x_2, x_3 axes; r_1, r_2, r_3 represent nodal position in x_1, x_2, x_3 axes, originating from the geometry center within the waveguide's cross-sectional shape; and v_1, v_2, v_3 donate the nodal velocity in three axes.

2.2. Extraction of physical characteristics for eigen-solutions

In the context of SAFE calculations, dataset consisting of physical characteristics is extracted from the eigen-solutions, i.e., frequency-discrete eigen-wavenumbers and corresponding eigenvectors, which will appear as each point in dispersion curves. Within each eigen-solution, the eigenvector that corresponds to each wavenumber, contains the particle displacement $\boldsymbol{U}$, for every FE node across the cross section of the waveguide. Derived from nodal displacement $\boldsymbol{U}$, physical characteristics representing dynamic properties, such as angular momentum $\boldsymbol{L}$ and power flow $\boldsymbol{P}$ are also considered.

Calculated from eigenvectors and nodal coordinates, three physical characteristics encompassing particle displacement $\boldsymbol{U}$, power flow $\boldsymbol{P}$ and angular momentum $\boldsymbol{L}$ were used as the nodal-based dataset to characterize the distinct guided wave modes. To faithfully depict the guided waves' mode shapes based on nodal physical characteristics, it's essential to fine tune the mesh for uniformity within the SAFE model. This guarantees an even sampling of the wave structures and the equitable utilization of nodal data.

Specifically, three types of field characteristics projected along x_1, x_2 and x_3 axes result in the extraction of nine-dimensional data for each FE node, as illustrated in Fig. 2. In the following notation, we use U, P, and L to denote the physical characteristics of nodal displacement, nodal velocity, and nodal power flow, respectively. Subscripts 1, 2, and 3 correspond to the coordinate axes, while superscripts m and i represent the mth frequency-discrete eigen-solution and the ith FE node, respectively. Consequently, the original dataset size becomes $N \times M \times 9$, where N is the total amount of discretized FE nodes, and M is the total amount of frequency-discrete eigen-solutions.

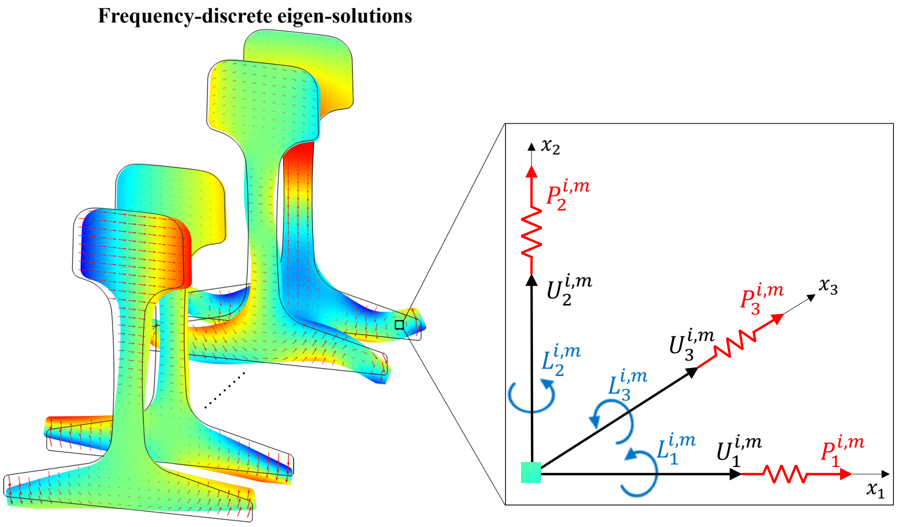

Figure 2: Illustrative diagram showing the physical characteristics extracted from the wave structure of a guided wave mode; multiple frequency-discrete eigen-solutions, i.e., eigen-modes, were derived from the SAFE calculations for an example railroad track; the FE nodal field characteristics U, P, and L projected along three orthogonal directions shown.

2.3. Distance measurement among eigen-modes

In this subsection, an enhanced cosine distance measurement and a weighted summation technique were utilized to evaluate the similarity of mode shapes across different frequency-discrete eigen-modes. These methods have played a crucial role in effectively reducing the dimensionality of the guided wave mode's field characteristics, compressing its original dataset, sized $N \times M \times 9$, along both the nodal indices and physical characteristics indices into a unified format. This streamlined process facilitates a more efficient and straightforward comparison among different eigen-solutions.

The complete distance measurement process, with the goal of obtaining the so-called distance matrix $\boldsymbol{D}$, is visually outlined in Fig. 3. To illustrate, when considering two frequency-discrete eigen-solutions

$\boldsymbol{m}, \boldsymbol{n}$, their physical characteristics along all three orthogonal directions were extracted and used to calculate the corresponding angular distance, i.e., $\theta_{X_r}(m,n)$, with X representing the field characteristic and r being coordinate axis, via the enhanced cosine distance measurement approach (detailed later). The weighted summation technique was then applied to condense the nine angular distances into one-dimensional distance, resulting in the (m,n)th entry of the distance matrix $\boldsymbol{D}$. By repeating this process for every pair of frequency-discrete eigen-solutions, the resultant distances are organized into a comprehensive distance matrix $\boldsymbol{D}$, serving as a pivotal input for constructing the subsequent similarity matrix.

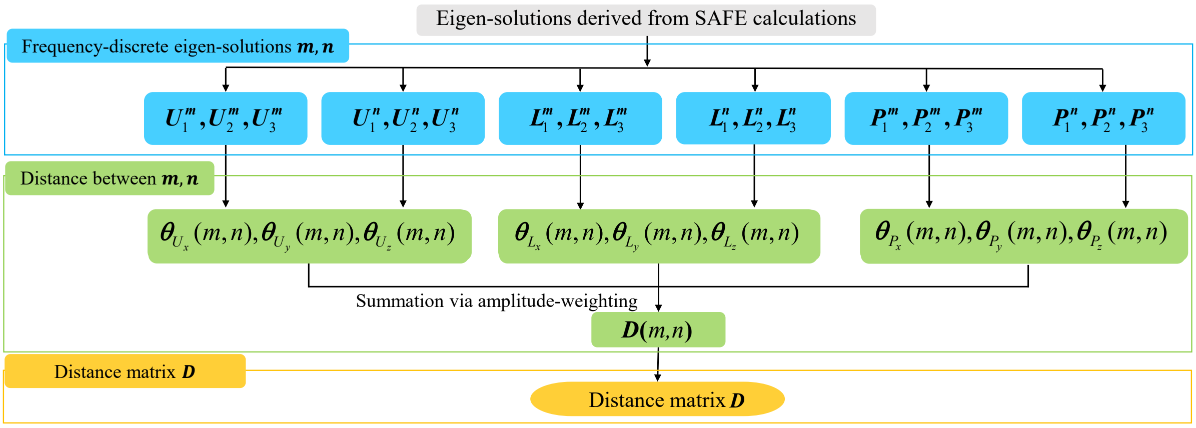

Figure 3: Flowchart showing the process of measuring the weighted cosine distances between any pair of eigen-solutions; the construction of distance matrix indicated.

We will start by explaining the principles of the enhanced cosine distance measurement technique. Mathematically speaking, cosine distance measurement quantifies the similarity between two vectors in a multi-dimensional space, commonly used in machine learning, data analysis, and signal processing. The cosine distance between two vectors, often represented as θ, is calculated by measuring the cosine of the angle between them. From the perspective of physics, the vectors typically denote various attributes of the guided wave modes, such as particle displacement, stress, power flow density, angular momentum, or other measurable quantities. The calculated cosine distance, based on the angle between these vectors, can provide a measure of their alignment or divergence in the corresponding physical features. Herein, to properly evaluate the alignment or dissimilarity of wave structures between different eigen-solutions, two key issues must be addressed: (1) handling the antiparallel eigenvectors encountered in the eigenvalue problem computation; and (2) executing a weighted summation over different physical characteristics.

To illustrate, using the given notations, each type of field characteristic along a specific axis is organized into an $N \times 1$ array encapsulating the corresponding mode shape in that direction. For instance, the nodal displacement for an eigen-solution $\boldsymbol{m}$ is represented as $\boldsymbol{U_1^m} = [U_1^{m,1}, U_1^{m,2}, ..., U_1^{m,N}]^T$, according to the FE nodal index. Similar arrays can be defined for such field characteristic in all the three axes. Whilst the direction calculation of cosine distance encounters "anitiparallel eigenvector" problem, i.e., cross-sectional numerical reversal of eigenvectors, as visualized in Fig. 4(a). This may arise from different initial phases due to the nature of numerical computations, or inherent symmetries in the system. Consequently, it will lead to invalid cosine distance measurements, and hence impede the accurate assessment of similarity between eigen-solutions. To adress this, we introduced a regulation approach that involves aligning the antiparallel eigenvectors to ensure these eigenvectors consistent and comparable.

When comparing two arrays of nodal displacement $\boldsymbol{U_1^m}$ and $\boldsymbol{U_1^n}$, belonging to different eigen-solutions, their cosine distance $\theta_{U_1}(m,n)$ can be defined as

$$\theta_{U_1}(m,n) = \begin{cases} arccos\left(\frac{\boldsymbol{U_1^m}\cdot\boldsymbol{U_1^n}}{\|\boldsymbol{U_1^m}\|\|\boldsymbol{U_1^m}\|}\right) & for\ \ 0 \leq arccos\left(\frac{\boldsymbol{U_1^m}\cdot\boldsymbol{U_1^n}}{\|\boldsymbol{U_1^m}\|\|\boldsymbol{U_1^m}\|}\right) \leq \frac{\pi}{2} \\ \pi - arccos\left(\frac{\boldsymbol{U_1^m}\cdot\boldsymbol{U_1^n}}{\|\boldsymbol{U_1^m}\|\|\boldsymbol{U_1^m}\|}\right) & for\ \ \frac{\pi}{2} < arccos\left(\frac{\boldsymbol{U_1^m}\cdot\boldsymbol{U_1^n}}{\|\boldsymbol{U_1^m}\|\|\boldsymbol{U_1^m}\|}\right) \leq \pi \end{cases}, \tag{5}$$

where "$\|\cdot\|$" is the Euclidean 2-norm of an array, and "$\cdot$" denotes the dot product of the two arrays. The optimized cosine distances for each field characteristic thus lie between 0 and $\pi/2$, and lower cosine angle signifies higher correlation between the frequency-modes' field characteristics. As schematically shown in Fig. 4(b), the cosine distance between nodal displacement $\boldsymbol{U_1^m}$ and other three frequency-modes' nodal displacements $\boldsymbol{U_1^n}$, $\boldsymbol{U_1^p}$, and $\boldsymbol{U_1^q}$ are compared. The cosine distance between $\boldsymbol{U_1^m}$ and $\boldsymbol{U_1^n}$ is close to 0, indicating their high correlation; the cosine distance between $\boldsymbol{U_1^m}$ and $\boldsymbol{U_1^p}$ is approximately $\frac{\pi}{2}$, denoting their low correlation. Aided by the regulation approach, despite exhibiting antiparallel attributes, nodal displacements $\boldsymbol{U_1^m}$ and $\boldsymbol{U_1^q}$ still obtain a calculated cosine distance approaching 0, affirming their high correlation.

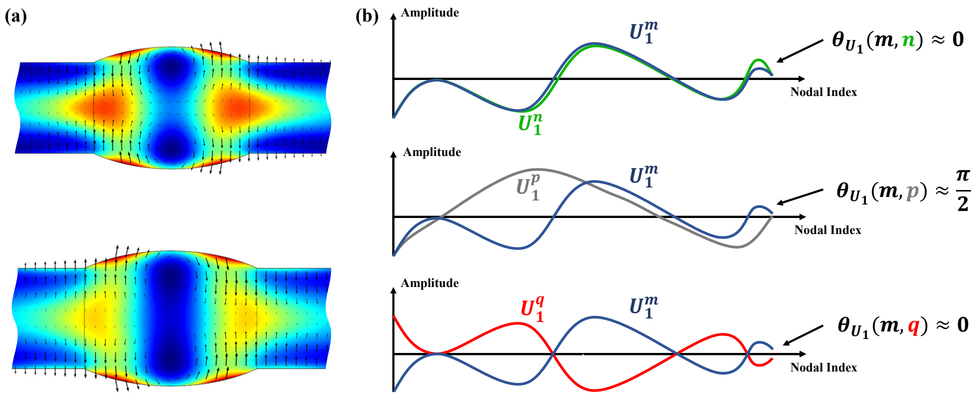

Figure 4: (a) Example wave structures for two eigen-solutions belonging to the same guided wave mode exhibit "anitiparallel eigenvector" phenomenon; arrows represent its particle displacement in the cross-section; color coding shows the distribution of the axial power flow in the waveguide (blue:low to red:high); (b) diagram illustrating the implementation of enhanced cosine distance measurement between eigen-solutions $\boldsymbol{m}$, $\boldsymbol{n}$, $\boldsymbol{p}$ and $\boldsymbol{q}$, regarding the nodal displacement $\boldsymbol{U_1}$.

Through enhanced cosine distance measurement, dimension reduction along the nodal index has been attained. Each type of field characteristic encompasses three dimensions, resulting in nine cosine distances between every pair of frequency-discrete eigen-solutions. To further condense the dimensions of physical characteristics and derive a scalar measure, an amplitude-weighting method was used. It initially calculates the absolute amplitude of the eigenvectors, which involves taking the absolute value of each component of the eigenvector. With the obtained absolute amplitudes, the weights are assigned for the field characteristics in all three axes between two frequency-discrete eigen-solutions. The combination of enhanced cosine distance with these weights results in an reduced dimenionality of physical characteristics. Specifically, as per nodal displacement, the average of the absolute amplitudes of eigen-solution $\boldsymbol{m}$ along each axis can be given by

$$\overline{U_r^m} = \frac{\sum_{i=1}^{N} |U_r^{m,i}|}{N},\ r = 1, 2, 3. \tag{6}$$

Likewise, the amplitude-weighting approach were applied to angular momentum L and power flow P in all three axes. Based on the average of absolute amplitudes for a single frequency-discrete eigen-solution, the amplitude weighting between two eigen-solutions $\boldsymbol{m}$ and $\boldsymbol{n}$ can be calculated as

$$W_{U_r}(m,n) = \frac{\overline{U_r^m} + \overline{U_r^n}}{\sum\limits_{s=1,2,3} (\overline{U_s^m} + \overline{U_s^n})},\ r = 1,2,3, \tag{7}$$

where the subscript U_r represents nodal displacement physical characteristic in specific direction. Similarly, we can define weights between two frequency-discrete eigen-solutions for angular momentum $W_{L_r}(m,n)$ and $W_{P_r}(m,n)$, respectively. It is worth noting that the summation of weights across all axes with corresponding characteristic quantities satisfies the normalization condition, which is expressed as

$$\sum_{r=1,2,3} W_{U_r}(m,n) = 1, \quad \sum_{r=1,2,3} W_{L_r}(m,n) = 1, \quad \sum_{r=1,2,3} W_{P_r}(m,n) = 1. \tag{8}$$

Considering that each physical characteristic among U, L, P is capable of independently characterizing guided wave propagation, without loss of generality, these weights are combined with the cosine distance for each field characteristic, and equal weights are assigned to these three type of physical characteristics. The resulting weighted distance $\theta(m,n)$ between two distinct frequency-discrete eigen-solutions can thus be expressed as the following summation

$$\theta(m,n) = \sum_{r=1,2,3} W_{U_r}(m,n)\theta_{U_r}(m,n) + W_{P_r}(m,n)\theta_{P_r}(m,n) + W_{L_r}(m,n)\theta_{L_r}(m,n), \tag{9}$$

where value of $\theta(m,n)$ falls within the range of $[0, 3\pi/2]$. Eqs. $(5 \sim 9)$ accomplish the dimension reduction through cosine distance measurements and assicated weight summation, effectively condensing the distance between two eigen-solutions to a scalar value.

It should be noted that the eigen-solutions derived at the same frequency are naturally orthogonal, their weighted cosine distance are prescribed as the maximum distance, i.e., $3\pi/2$. Such prescription regarding $D(m,n)$ can be expressed as

$$D(m,n) = \begin{cases} \frac{3}{2}\pi \quad, f_m \neq f_n \\ \theta(m,n), f_m = f_n \end{cases}, \tag{10}$$

where f_m and f_n denote the discrete frequencies for eigen-solutions $\boldsymbol{m}$ and $\boldsymbol{n}$, respectively.

While the cosine distance measures differences in guided waves' mode shapes, the weighted summation over cosine distances are rooted in fundamental physical principles governing the guided wave propagation. The utilization of amplitude-weighting approach actually conforms to the facts that the components of particle displacement, stress, angular momentum, and power flow along specific directions are often dominant in the wavefield of guided wave modes, which should be considered more influential or significant in the assessment of similarity or dissimilarity between eigen-solutions.

2.4. Construction of similarity matrix via similarity propagation

In this subsection, we utilize the similarity propagation technique involving the transfer or propagation of similarity information between frequency-discrete eigen-solutions, generating the similarity matrix $\boldsymbol{S}$. This matrix serves as the input for the Affinity Propagation (AP) clustering algorithm. The initial state of the similarity matrix $\boldsymbol{S}$ is set as $\boldsymbol{S} = -\boldsymbol{D}$, in which the higher values of $\boldsymbol{S}(m,n)$ suggest a greater likelihood of clustering the corresponding eigen-solutions into the same guided wave mode.

As per a specific guided ultrasonic wave mode, its mode shape among the investigated frequency range will change gradually with the increasing frequency, which stems from the interaction and interference between the elastic waves of varying wavelengths and the waveguide's boundaries. Such frequency-dependent variations in wave structure becomes even pronounced in waveguides with complex cross-sectional shapes and/or intricate boundary conditions, as well as in open-waveguide systems. Consequently, the solved eigen-solutions, e.g. $\boldsymbol{m}$ and $\boldsymbol{n}$, even belonging to the same guided wave mode, may exhibit substantial variations in mode shape at frequencies that are significantly distant on the frequency axis, thus leading to a considerable distance $D(m, n)$. To address this, a similarity propagation technique [37] based on the shortest paths or distances was used. Its main idea is to link eign-solutions that are most similar or share the shortest distance, assuming that such connections represent clusters within the dataset. The utilization of the similarity propagation technique assists in identifying patterns and groupings in dataset to form clusters in a way that minimizes the overall distances between all the connected eigen-solutions within each cluster while maximizing the difference between clusters. This choice is motivated by the need to capture the nuanced relationships between eigenvectors exhibiting tolerable differences.

Similarity propagation can be implemented via neighborhood establishment and transferring similarity information. Fig. 5 schematically illustrates the process of neighborhood establishment, linking the frequency-discrete eigen-solutions through a series of neighborhood relations. Fig. 5(a) shows part of the phase velocity dispersion curves of guided wave modes in an 8-layer composite plate, derived from the heterogeneous SAFE modelling (detailed in Section3.1). The wave structures corresponding to the same guided wave modes, i.e., eigen-solutions $\boldsymbol{m}$, $\boldsymbol{n}$, $\boldsymbol{r}$, $\boldsymbol{s}$, and those corresponding to different guided wave modes, i.e., eigen-solutions $\boldsymbol{p}$, $\boldsymbol{q}$ are visualized. These frequency-discrete eigen-solutions are also depicted in the high-dimensional feature space, as shown in Fig. 5(b). We introduced a neighborhood size designated as H that defines the distances or proximity within which neighboring eigen-solution points are considered relevant to the given point. In the high-dimensional feature space, which is nine-dimensional in this study, the neighborhood region, characterized by a radius, i.e. neighborhood size, and centered around each eigen-solution point, is visualized as a red hypersphere. Specifically, the weighted cosine distance between eigen-solution points $\boldsymbol{m}$ and $\boldsymbol{n}$ is $D(m, n)$, and the $D(n, r)$ and $D(r, s)$ denote the distances between the eigen-solution points $\boldsymbol{n}$ and $\boldsymbol{r}$, and $\boldsymbol{r}$ and $\boldsymbol{s}$, respectively. For instance, as per the eigen-solution point $\boldsymbol{m}$, three potential candidate points $\boldsymbol{n}$, $\boldsymbol{p}$, and $\boldsymbol{q}$ obtained at adjacent frequency can be considered to be affiliated to the same guided wave mode; and both points $\boldsymbol{n}$ and point $\boldsymbol{q}$ fall within its neighborhood region with a radius of H_m, while the point $\boldsymbol{p}$ does not. Furthermore, point $\boldsymbol{n}$ possesses the closest distance, i.e., $D(m, n) < H_m$, to point $\boldsymbol{m}$, resulting in the establishment of a neighborhood relation between points $\boldsymbol{m}$ and $\boldsymbol{n}$, as indicated by the solid arrows in Fig. 5(b).

Upon the neighborhood establishment, the transferring of similarity information has to be implemented sequentially along the frequency axis. Through this technique, the eigen-solutions possessing dissimilar mode shapes at distant frequencies, can still achieve a neighborhood relation, provided that multiple inter-points in the investigated frequency range are connected in a chain-like manner with such neighborhood relations. The associated implementation procedures are outlined in Fig. 6.

The neighborhood matrix $\boldsymbol{N}$ is defined herein to explicitly represent the above-mentioned neighborhood relations. Specifically, $\boldsymbol{N}(m, n) = 1$ if points $\boldsymbol{m}$ and $\boldsymbol{n}$ keep a neighborhood relation; otherwise, $\boldsymbol{N}(m, n) = 0$. The propagation process involves finding all possible paths connecting each pair of frequency-discrete eigen-solutions, as depicted in Fig. 6. If points $\boldsymbol{m}$ and $\boldsymbol{n}$ lack a neighborhood relation, all points that have a neighborhood relation with either $\boldsymbol{m}$ and $\boldsymbol{n}$ are examined to identify a possible path connecting points $\boldsymbol{m}$ and $\boldsymbol{n}$. Once such propagated neighborhood relation is attained through

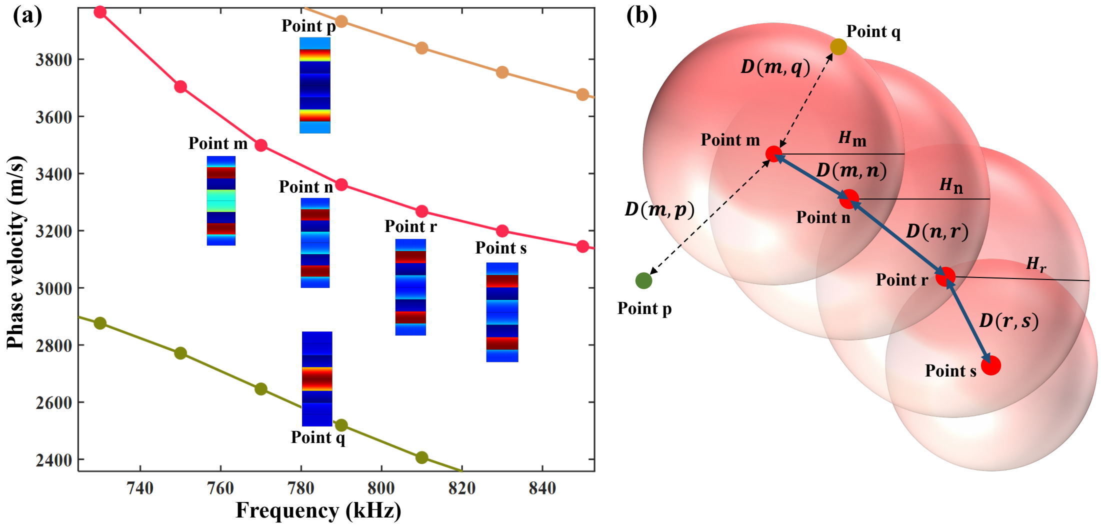

Figure 5: Schematics illustrating the process of neighborhood establishment: (a) dispersion curves of guided wave modes in a heterogeneous composite plate (detailed in Section 3.1), with frequency-discrete eigen-solution points $\boldsymbol{m}$, $\boldsymbol{n}$, $\boldsymbol{r}$ and $\boldsymbol{s}$ belonging to the same mode; the color coding represents the through-thickness distribution of axial power flow of guided wave modes; (b) visualization of linking the corresponding eigen-solution points through a series of neighborhood relations in the feature space; the neighborhood regions depicted by red hyperspheres; the established linkage denoted by double-headed arrow line.

point $\boldsymbol{p}$, the similarities among points $\boldsymbol{m}$ and $\boldsymbol{n}$, and the newly connected point $\boldsymbol{p}$ will be assessed, and the maximum similarity value within this connectivity path will be taken as the $S(m,n)$. Such procedure will be repeated for every pair of eigen-solutions $(\boldsymbol{m},\boldsymbol{n})$, following the sequences that $m : 1 \sim M$ and $n : (m+1) \sim M$. Revisiting Fig. 6(b), points $\boldsymbol{s}$ and $\boldsymbol{m}$, despite outside each other's neighborhood region, have a propagated neighborhood relation due to the sequential connections of neighborhood relations between point m and n, n and r,and r and s. Therefore, the similarity value $S(m,n)$ between point $\boldsymbol{m}$ and $\boldsymbol{s}$ will be updated according to Fig. 6.

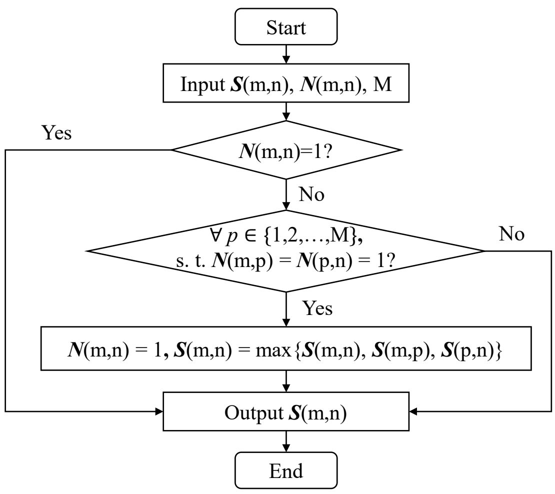

Figure 6: Illustrative flowchart for the implementation of similarity propagation.

As evident in the above mentioned process of similarity propagation, the setting of neighborhood size impacts the quality of the constructed similarity matrix S and hence clustering results. Physically, the guided wave modes are generally dispersive and the associated wave structures varying with frequencies, thus necessitating frequency-dependent neighborhood size to ensure the accuracy of the mode-tracing results. Herein, neighborhood size can be expressed as polynomials with respect to frequency. For the ease of implementation, without loss of generality, the neighborhood size $H(f)$ is set in the form of a linear function

$$H(f) = b + k(f - f_c), \tag{11}$$

where f denotes varying frequency; f_c represents the mean frequency across the investigated frequency range; and k is the slope and b is the predetermined intercept. Both the intercept neighborhood size b and the adjustment item kf_c take values in the range of [0,1]. The value of b is relevant to the complexity of the guided wave system, and the value of k is related to the frequency span in the mode-tracing problem. The associated parameter selection will be discussed in detail in Section 4.1.

2.5. Affinity propagation clustering

Having assessing the similarity matrix $\boldsymbol{S}$ based on the distance matrix $\boldsymbol{D}$ and neighborhood matrix $\boldsymbol{N}$, the subsequent step utilizes the Affinity Propagation (AP) clustering algorithm [38] to process the similarity matrix $\boldsymbol{S}$. This algorithm is employed to cluster the eigen-solutions, ultimately yielding the mode-tracing results.

The AP clustering method uses similarities $\boldsymbol{S}$ between each pair of eigen-solutions as inputs, considering all the eigen-solutions as candidate exemplars. Throughout the clustering process, two kinds of real-valued messages encompassing "responsibility" and "availability" are iteratively updated and exchanged between eigen-solutions until a high-quality set of exemplars and corresponding clusters gradually emerges. These messages can be combined at any stage to decide which eigen-solutions serve as exemplars and, for every other eigen-solution, which exemplar it belongs to, such that the tracing of guided wave modes resembles an iterative "voting" process. Importantly, the AP clustering thus doesn't require the predetermined the number of clusters, offering greater flexibility, which is different from the commonly-utilized K-means clustering algorithm.

The associated implementation procedures are visually outlined in Figure 7. As per any pair of eigen-solutions $\boldsymbol{i}$ and $\boldsymbol{k}$, the"responsibility" $\boldsymbol{R}(i,k)$, sent from eigen-solution $\boldsymbol{i}$ to candidate exemplar eigen-solution $\boldsymbol{k}$, represents the accumulated evidence for how well-suited eigen-solution $\boldsymbol{k}$ is to serve as the exemplar for eigen-solution $\boldsymbol{i}$ in comparison to other potential exemplars. The "availability" $\boldsymbol{A}(i,k)$ sent from candidate exemplar eigen-solution $\boldsymbol{k}$ to eigen-solution $\boldsymbol{i}$, reflects the accumulated evidence for how appropriate it would be for eigen-solution $\boldsymbol{i}$ to choose eigen-solution $\boldsymbol{k}$ as its exemplar, considering the support from other eigen-solutions that suggest $\boldsymbol{k}$ should be an exemplar. In the beginning, the initialization is set as $\boldsymbol{A}(i,k) = 0$ and $\boldsymbol{R}(i,k) = 0$; and the diagonal elements of the similarity matrix $\boldsymbol{S}$ are set as "preference" parameter p, which is determined as the median of the input similarities according to Eq. (12), resulting in a moderate number of clusters [38].

$$p = \frac{\sum\limits_{i=1}^{M}\sum\limits_{k=1}^{M} \boldsymbol{S}(i,k)}{M \times M}, \tag{12}$$

where M is the total amount of frequency-discrete eigen-solutions in the investigated frequency range.

To summarize the methodology, the utilization of the enhanced cosine distance measurement combined

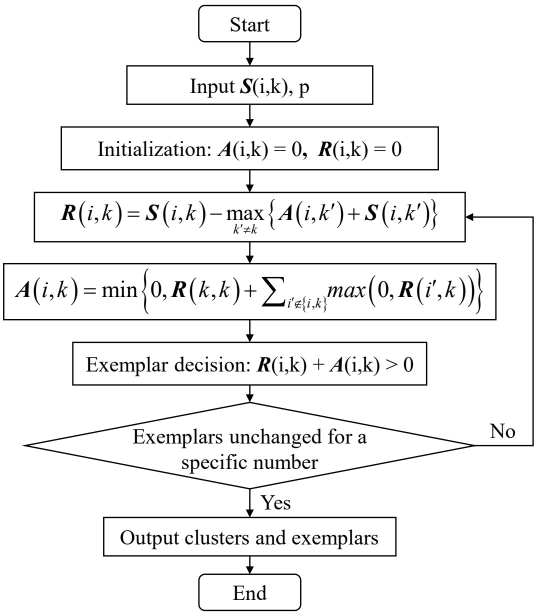

Figure 7: Procedures for implementing the AP clustering algorithm; two types of real-valued messages "responsibility" and "availability" denoted.

with weighted summation technique effectively evaluates the distance matrix $\boldsymbol{D}$ among frequency-discrete eigen-solutions. Through the similarity propagation, the similarity matrix $\boldsymbol{S}$ is then well-constructed based on the matrix $\boldsymbol{D}$. The physics-driven AP clustering algorithm can thus be executed to generate the clusters, i.e., the tracing results of guided wave modes.

3. Numerical examples of Relevance to NDE/SHM interests

3.1. Guided waves in anisotropic viscoelastic plates

To validate the effectiveness of proposed automated mode-tracing technique, we initially apply the algorithms to guided wave modes in an example viscoelastic composite plate. This serves as a proof-of-concept study for utilizing sparse frequency-discrete eigen-solutions to derive dispersion curves. Employing two main modeling approaches for composite plates, encompassing homogeneous and heterogeneous models, allows us to assess the versatility of such technique in the given scenario for the multi-layered media.

The composite plate is made of eight carbon epoxy plies with a quasi-isotropic layup $[0/45/90/\text{-}45]_s$, and its stacking thickness is 1.6 mm and the mass density is 1.58 kg/m^3. The viscoelastic moduli were measured by a well-established ultrasonic technique [39], and are presented in Table 1, which serve as the inputs for homogeneous SAFE modelling. The reference coordinate system to define fibrous materials is set such that the fibrous lie along the x_3 axis and the layer interfaces are normal to the x_1 axis. Additionally, the effective complex stiffness matrix for corresponding unidirectional stacking essential for heterogeneous SAFE modelling, is also measured and detailed in Table 2. Alongside this, the fiber orientations throughout the plate thickness were assigned accordingly.

Table 1: The homogenized viscoelastic moduli of the studied composite plate (in GPa).

C_{11}	C_{12}	C_{13}	C_{22}	C_{23}	C_{33}	C_{44}	C_{55}	C_{66}
13.1+0.4i	7.0+0.11i	7.0+0.11i	63.7+3.1i	20.4+0.8i	63.7+3.1i	21.6+0.86i	3.9+0.11i	3.9+0.11i

Table 2: The viscoelastic moduli of the unidirectional composite plies for heterogeneous modeling (in GPa).

C_{11}	C_{12}	C_{13}	C_{22}	C_{23}	C_{33}	C_{44}	C_{55}	C_{66}
13.1+0.4i	6.8+0.12i	7.1+0.05i	13.8+0.37i	4.7+0.01i	145+7.8i	5.9+0.04i	5.2+0.36i	3.1+0.01i

Through the SAFE calculations across the frequency range from 50 kHz to 1 MHz, the eigen-solutions at discrete frequencies were obtained from both homogeneous and heterogeneous modeling. As shown in Fig. 8(a), upon utilizing the proposed AP clustering technique, these eign-solutions have been automatically grouped into six clusters, representing the successfully traced dispersion curves for guided wave modes, i.e., S0, SH0, A0, S1, SH1, A1 modes, propagating along the 0° fibre direction in the composite plate. The accuracy of the mode tracing results has been well validated by those obtained via the well-known "*Disperse*" software. In this case study, even dealing with the eigen-solutions derived at a much coarser frequency discretization, e.g., three times frequency step, the correctness of the tracing results remained robust. Noteworthily, as evident in Fig. 8(b), the wave structures derived from heterogeneous and homogeneous modeling showcase distinct spatially-varying features across the plate thickness. It can be predicted that the utilization of the proposed method is capable of capturing both physics-informed features in multi-layered media, thus generating accurate tracing result.

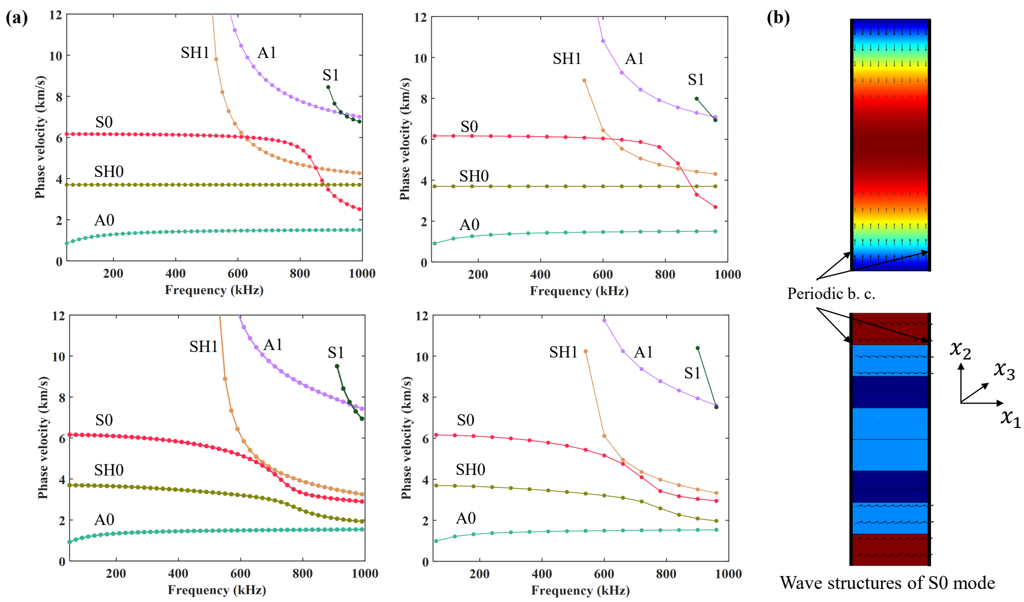

Figure 8: (a) Mode tracing results for guided waves in a carbon epoxy composite plate; the upper and the lower represent the well-traced dispersion curves for homogeneous and heterogeneous SAFE calculations respectively; varied frequency discretization size of 20 kHz and 60 kHz used; (b) wave structures of the S0 mode derived from homogeneous and heterogeneous modeling at 50 kHz, showing different multi-layered features.

3.2. Guided waves in closed bars of arbitrary cross-sections

The purpose of this section is to demonstrate the applicability of the AP clustering to the guided wave problem regarding closed waveguides of arbitrary cross-sections. The case treated is that of a steel railroad track, considered as a typical 115-lb A.R.E.M.A. section, which had been studied in Ref. [20] and its material properties are replicated herein as: $\rho = 7932\ kg/m^3$, $V_L = 5960\ m/s$ and $V_S = 3260\ m/s$. Accurate knowledge and mode tracing of their guided waves' dispersive behavior is relevant for the purpose of long-range screening of defects in rails up to 50 kHz [40].

In the SAFE calculation, the cross-section of the rail was meshed by 7416 quadratic Lagrangian triangular elements, consisting of 3910 FE nodes. In total, 1589 frequency-discrete eigen-solutions were obtained in the frequency range from 5 kHz to 50 kHz, with the discretization size of 0.5 kHz. The dispersion results are shown in the Fig. 9(a), and totally 31 guided wave modes has been traced in the railroad track. The correctness of the mode-tracing results was verified by those identified manually in Ref. [20]. Such tracing process was accomplished via the AP clustering algorithms through 35 iterations within a span of 5 minutes, utilizing the computational power of an i7 11800H CPU with 16GB RAM.

Additionally, as indicated by the dispersion curves, the "mode-veering" phenomenon in this scenario has been properly accommodated, where two or more guided wave modes exhibit a change in their propagation characteristics such as phase velocity, group velocity, or mode shape, and associated interactions and interferences cause them to veer towards or diverge from each other. Such phenomenon can occur due to various factors, including geometric irregularities, material heterogeneities, or changes in the structural boundary conditions [28]. As illustrated by the zoomed-in dispersion curves for the mode 5 and mode 7 in Fig. 9(a), they approach and move away from each other in the frequency vicinity of 20 kHz. The corresponding wave structures, comparatively depicted in Fig.9(b), showcase distinct mode shapes and distributions of power flow density. It can be seen that mode veering poses challenges in identifying and analyzing the adjacent guided wave modes in their phase/group velocity dispersion curves. Nevertheless, the proposed clustering technique is capable of capturing and dealing with this problem, owing to the physics-informed data acquisition. This capability potentially allows us to handle a great amount of guided wave modes in complex guided wave problems.

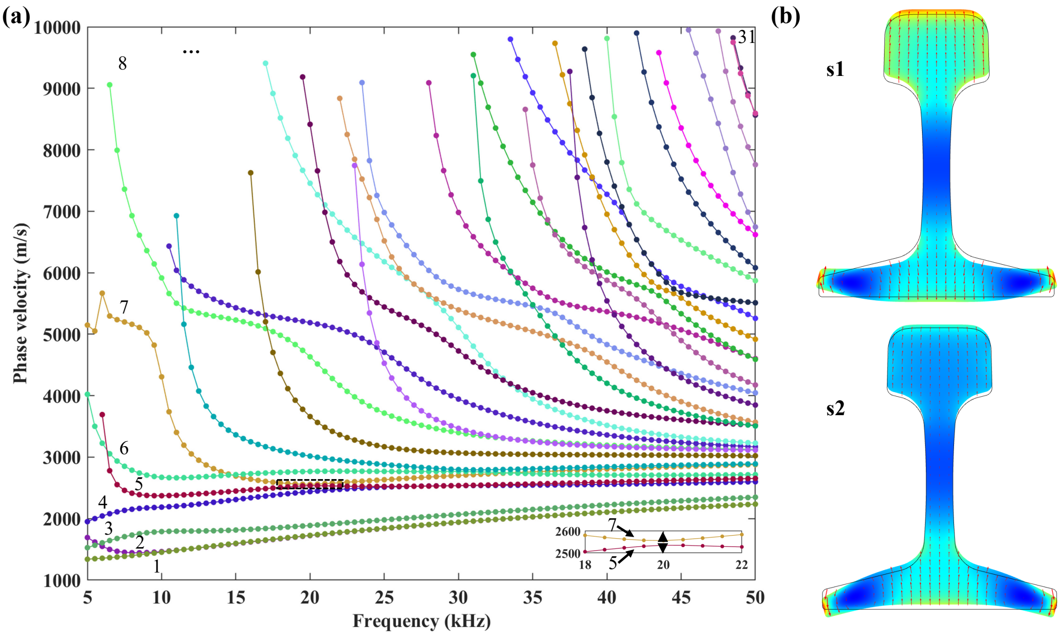

Figure 9: (a) Successfully traced dispersion curves of guided wave modes in the railroad track; 31 clusters of guided wave modes are distinguished by color; the "mode-veering" phenomenon exemplified by modes 5 and 7 shown in the zoom-in image; (b) cross-sectional visualization of wave structures for two adjacent guided wave modes: ▲, wave structure s1 of mode 7; ▼, wave structure s2 of mode 5 at 20kHz.

3.3. Feature guided waves in transversely-unbounded welded joints

In closed waveguides, as exemplified in Section 3.2, guided wave modes can propagate along the guide axis without attenuation in non-dissipative media. However, in practical engineering structures, waveguides are often embedded in large solid media that can be considered as unbounded. In this regard, such guided wave propagation system are referred to as "open wave guided problem" due to the possible energy radiation into the surrounding medium. A particular branch of guided waves, confined to the extended plate-like structures with local geometry or/and material variation, such as welds [41], stiffeners [42] and bends [43], have been discovered as feature guided waves (FGW), rendering the energy of the elastic waves preferentially transmitted along structural features with very limited energy leakage into the adjacent parent plates.

In this subsection, the tracing of guided wave modes in an example transversely-unbounded steel welded plate, was performed using the AP clustering to demonstrate its effectiveness in handling such open waveguide scenarios. The thickness of the parent steel plate is 10 mm, and the height and the width of the weld region are 13.46 mm and 17.2 mm, respectively. Through the SAFE calculation of guided wave modes in welded joints that had been studied in Ref. [44], the physical characteristics were extracted from 688 FE nodes across the cross-section of the weld feature region, and totally 555 FGW frequency-discrete eigen-solutions were identified in the frequency range from 50 kHz to 700 kHz, with a frequency step of 10 kHz. Through 35 iterations by the AP clustering, 20 clusters have been emerged as the phase velocity dispersion curves shown in Fig. 10(a). Their attenuation ratio spectrum is accordingly attained in Fig. 10(b). These tracing results are consistent with those that were derived manually in the literature and were broadly categorized into four wave families based on their wave structures, encompassing the shear horizontal (SH) type, the flexural (F) type, the longitudinal (L) type and the torsional (T) type modes, as depicted respectively in Fig. 10(c).

It can also be observed in Fig 10(a) that certain FGW modes, e.g., modes 1 and 2, were found to preserve missing frequency breaking-up band, occurring at locations which the velocities of the modes equal to that of either the bulk shear wave or the Rayleigh wave. As the phase velocity of FGWs goes around these values, the energy can not be trapped in the weld feature region and the eigen-solutions will vanish at these points, only to reappear a few frequencies later. Such "piece-wise" phenomenon can be well dealt with using the AP clustering approach, but the traced discontinuous dispersion curve has been taken as two different clusters due to the relatively large difference in their wave structure.

3.4. Feature guided waves in adhesively bonded skin-stiffener composite joints

This section presents SAFE results of guided wave modes in stiffener-bond-skin composite structures, which are commonly encountered in aerospace engineering. The composite assembly consists of a T-shaped aluminum stiffener, a viscoelastic orthotropic CFRP composite plate, and a viscoelastic isotropic adhesive layer, and their material properties are replicated in Table.3 [45]. The associated feature thicknesses are 1.6 mm, 0.75 mm and 1.6 mm. Totally 228 FGW frequency-discrete eigen-solutions were derived from the SAFE calculations covering the frequency range from 50 kHz to 300 kHz, with a discretization step of 10 kHz. Through 41 iterations by the AP clustering, 20 clusters have been well-traced and appeared as the dispersion curves shown in Fig. 11(a), and the corresponding attenuation ratio spectrum is accordingly achieved in Fig. 11(b). These tracing results have been partially validated by those that had been identified via manual routines in the literature [45], across the frequencies from 50 kHz to 200 kHz.

The tracing results also reveal much more number of clusters that exhibit piece-wise characteristics in their dispersion curves. It can be observed that there exists upper or lower frequency limits as per these "piece-wise" guided wave modes, at which the velocities of the modes equal to that of the bulk longitudinal wave in the aluminum stiffener or that of the $SH0$ guide wave in the composite plate. For

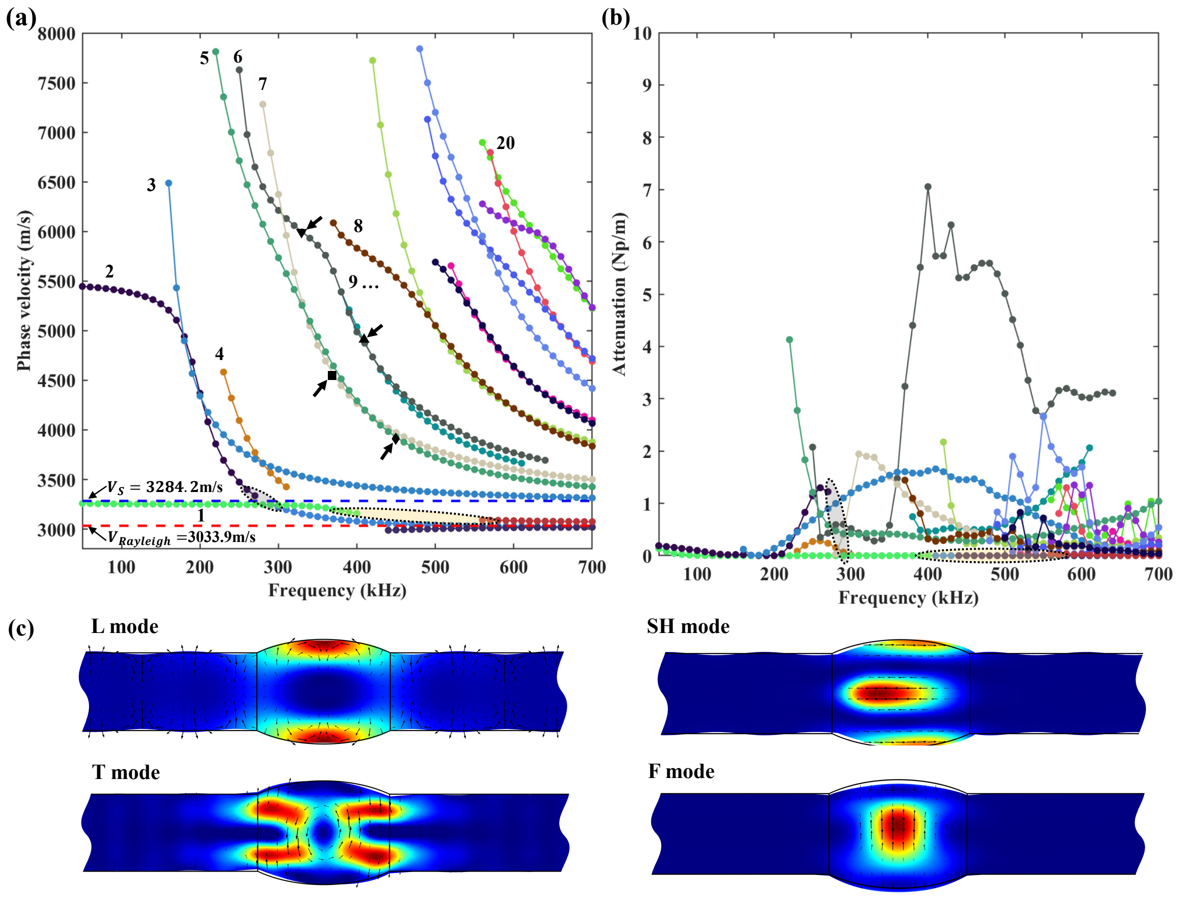

Figure 10: Mode tracing results for the guided waves confined to the weld beam in an open waveguide problem: (a) phase velocity and (b) attenuation dispersion curves; in total 20 clusters were identified, representing 18 physical propagative guided wave modes, and the disconnection regimes are highlighted by dotted ellipses; (c) typical cross-sectional wave structures for four types of weld-guided wave modes at particular frequencies: ▼, L-type, mode 6 at 330kHz; ■, SH-type mode 7 at at 370kHz; ▲, T-type mode 9 at 400kHz; ⧫, F-type mode 5 at 450kHz.

example, the traced mode 7 merely come into existence from 90 kHz to 110 kHz, and its evolution in the wave structure is shown in Fig. 11(c). It can be seen that as the frequency increases, the energy concentration area gradually transits from the upper beam portion of the stiffener to its bottom flange and then into the adhesive layer, eventually vanishing. The utilization of the proposed AP clustering method actually has aided in identifying and meanwhile tracing more guided wave modes in intricate waveguide problems.

3.5. Guided waves in waveguides with arbitrary prestress

Nondestructive evaluation of prestresses such as applied or residual stress in engineering structures is essential in that such stress status significantly impacts their mechanical responses. Acoustoelastic effect, which correlates the changes in the elastic wave velocity to a given stress field, potentially provides an attractive capability to measure prestress non-destructively. Unlike bulk waves, the acoustoelastic behavior of guided waves is frequency and mode dependent [46]. The present SAFE-Prestress modal study, which had been reported earlier in Ref. [47], is set within the framework of weakly nonlinear elasticity theory, intended for guided wave propagation in prestressed stiff solids. And the solved eigen-solutions will showcase the anisotropic changes in dispersion relations for various applied stresses.

Table 3: The material proprieties (in GPa) of the bonded skin-stiffener study

C_{11}	C_{12}	C_{13}	C_{22}	C_{23}	C_{33}	C_{44}	C_{55}	C_{66}
CFRP plate ($\rho = 3700\ kg/m^3$)								
13.1+0.4i	7.0+0.1i	7.0+0.1i	63.7+3.1i	20.4+0.8i	63.7+3.1i	21.6+0.86i	3.9+0.11i	3.9+0.11i
Adhesive layer ($\rho = 1050\ kg/m^3$)								
5.6+0.5i	4.5+0.4i	4.5+0.4i	5.6+0.5i	4.5+0.4i	5.6+0.5i	0.5+0.05i	0.5+0.05i	0.5+0.05i
Aluminum stiffener ($\rho = 1580\ kg/m^3$)								
107.84	54.76	54.76	107.84	54.76	107.84	26.54	26.54	26.54

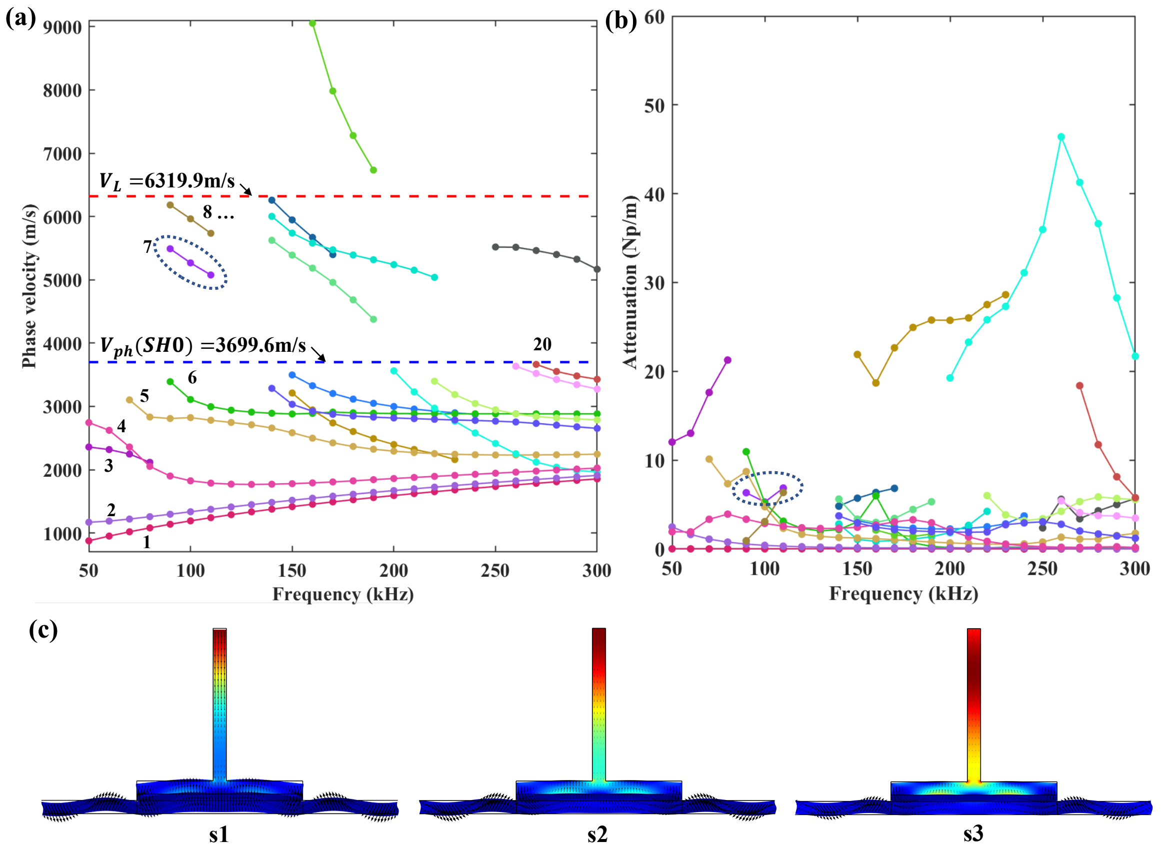

Figure 11: Outcomes of mode tracing for guided waves confined to the stiffener-bond-skin composite structures: (a) phase velocity and (b) attenuation dispersion curves investigated in the frequency range from 50 kHz to 300 kHz; the “piece-wise” phenomenon exemplified by the mode 7 is circled; (c) wave structures s1, s2 and s3 corresponding to the mode 7 at 90kHz, 100kHz and 110kHz respectively, with evolving power flow distribution.

This subsection aims to manifest the applicability of the proposed method in clustering the guided wave modes in pre-stressed waveguides. Besides variations in their wave structures and phase/group velocities, the prestresses can also lead to the “mode splitting” phenomenon, which refers to the guided wave modes split and form into two continuous modes original point of intersection from the unstressed case upon a stress is applied. This will introduce significant uncertainty or ambiguity into the manual mode-tracing process, thus inevitably necessitating an exceptionally fine frequency discretization size.

We performed the SAFE-Prestress calculations for the guided waves in an example 1 mm thick aluminum plate, which propagates at an angle of 45° to the direction of an applied uniaxial load of 100 MPa. Its equivalent SAFE configuration is shown in Fig. 12(a). This case had been analytically studied and manually traced in the Ref. [46] and its material properties encompassing the second and third order elastic constants are listed in Table. 4, Fig. 12(b) presents the SAFE results consisting of 318 eigen-solutions, grouped into 7 guided wave modes via the AP clustering, in the investigated frequency

Table 4: Material properties used for the 6061-T6 aluminum in the SAFE calculation [46].

ρ^0 (kg/m^3)	λ (GPa)	μ (GPa)	l (GPa)	m (GPa)	n (GPa)
2704	54.308	27.174	−281.5	−339	−416

range from 3300 kHz to 3750 kHz. As reported in the literature, the dispersion curves of the SH0 and S0 modes, under unstressed state, intersect at the vicinity of frequency of 3500 kHz. Whereas, it can be seen from Fig. 12(b) that the SH0 and S0 modes split at the original intersection frequency and were traced into two new guided wave modes under the stressed load, and their wave structures are very similar to each other. It is utilization of the similarity propagation along the frequency axis that had aided the accurate tracing of these two guided wave modes.

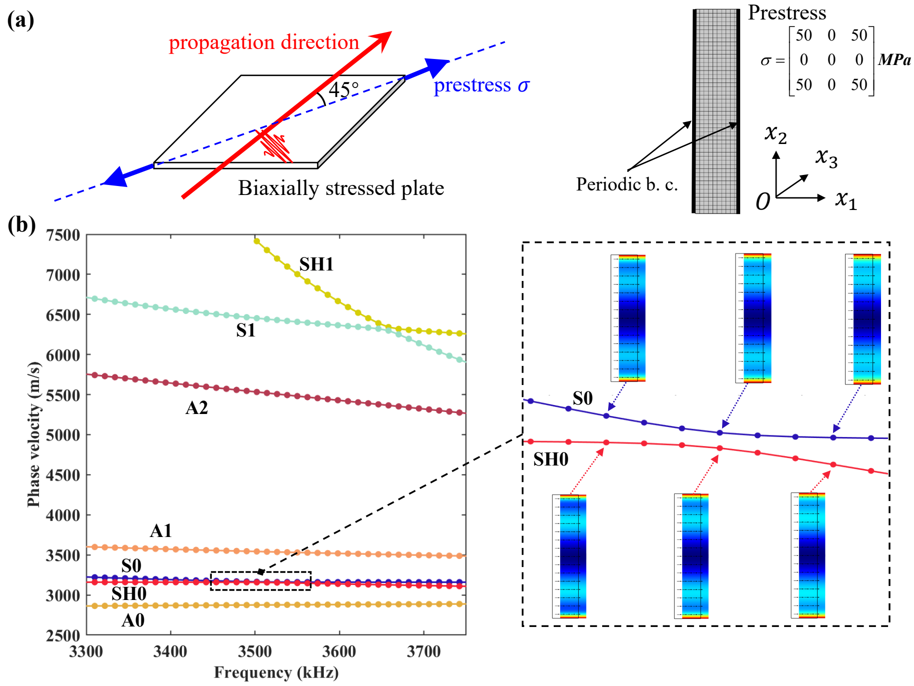

Figure 12: (a) Diagrams showing the guided wave propagation in a plate at an angle of 45° relative to the prestress σ and the corresponding SAFE-Prestress model with equivalent load; (b) the mode tracing results with frequency discretization size of 12 kHz, with zoomed-in dispersion curves of S0 and SH0 modes at around 3500 kHz to showcase the "mode splitting" phenomenon.

The intricate dispersion relations inherent to the complicated guided wave systems including mode veering, mode splitting and leaky modes necessitate much finer frequency discretization, for accurately capturing and tracing these dispersion curves. This motivate us to investigate the influence of varying frequency steps on the performance of the AP clustering, which will be discussed in detail in Section 4.2.

4. Discussions and recommendations

In this section, factors affecting the performance of the proposed AP clustering are discussed to enhance its practical applicability. The first aspect focuses on assessing the influence of neighborhood size on clustering results, employing the F-measure criterion as an evaluative benchmark. The second facet delves into the correlation between the selected frequency discretization size and the distribution of elements in the similarity matrix $\boldsymbol{S}$, ultimately determining the accuracy of mode tracing. The rationale behind the choice of these two crucial parameters is suggested as well.

4.1. Effects of neighborhood size

The frequency-dependent neighbourhood size $H(f)$, with the prescribed intercept b and slope k, is essential in the process of the AP clustering, and its values are relevant to the complexity of the studied guided wave system. The optimized $H(f)$ for all the cases studied in Section 3 is summarized in Table 5. Starting from the definition of the similarity matrix, the range of $H(f)$ is [0,1]. A relatively low value of $H(f)$ will be used for regular waveguides like plates or cylinders. However a relatively high value of $H(f)$ would be proper for complex guided wave systems to adapt to the guided modes' significant variations or fluctuations in wave structure, often accompanying highly dispersive characteristics.

Table 5: The neighborhood size selection for the delivered numerical examples.

Example waveguides	Intercept b	Adjustment item kf_c
Anisotropic viscoelastic plate	0.2	0
Railroad track	0.65	0.1
Unbounded welded joint	0.45	0.2
Adhesively composite joint	0.45	0.05
Arbitrary prestressed plate	0.3	0.15

As the selection of the neighborhood size $H(f)$ would affect the tracing results, the classical F-measure criterion was introduced in this subsection as a quantifiable metric to evaluate the accuracy of mode tracing. Specifically, we designate the cluster derived by the AP clustering as C_x, and refer to the cluster of ground truth as C_k. Let N_{xk} be the number of eigen-solutions simultaneously encapsulated in both clusters C_x and C_k; and N_x and N_k denote the number of eigen-solutions in cluster C_x and C_k, respectively. The precision (P) and the recall (R) can be calculated as $P = N_{xk}/N_k$, and $R = N_{xk}/N_x$ [48]. Thus, the F-measure between these two clusters can be obtained as $F_{xk} = 2PR/(P + R)$ [49]. Furthermore, in order to assess the accuracy of overall mode-tracing results, the total F-measure F_{total} between the predicted and the actual groups of clusters, i.e., the traced guided wave modes, can be obtained as

$$F_{total} = \sum_{x \in X} \frac{N_k}{N} \max_{k \in K} (F_{xk}), \tag{13}$$

where X is the number of clustered guided wave modes predicted by the AP clustering; K denotes the number of actual clusters of guided wave modes; and N represents the total amount of frequency-discrete eigen-solutions. The range of the F_{total} is [0,1], and the higher the value of F_{total}, the more accurate the tracing results.

To further assess the robustness of the AP clustering method, a parametric study was carried out by sweeping b and kf_c by $\pm 50\%$ separately from their currently-adopted values, and the robustness results are depicted in Fig. 13. It can be observed that there is barely no loss in accuracy of tracing guided wave modes in the railroad track, while the F-measure of the traced clusters of guided wave modes in the unbounded welded joint and in the adhesively composite joint drops up to 18% and 10% respectively for such variations in b and kf_c. Meanwhile, as evident by the varied distribution of F-measure along the b and kf_c axes, the intercept b executes relatively significant influence on the clustering results compared to the adjustment item kf_c.

Herein, we followed the "k-nearest-neighbor rule" proposed in the Ref. [50] and utilized a linear form function of $H(f)$ (as described in Section 2.5) to ensure a consistent number of candidate eigen-solutions in the neighborhood range for each frequency-discrete eigen-solution across the investigated frequency range. It can be concluded that $b + kf_c$ should be smaller than the absolute mean value of the elements in similarity matrix S. Empirically, the intercept b range [0.2, 0.4] and the adjustment item kf_c range [0,0.1]

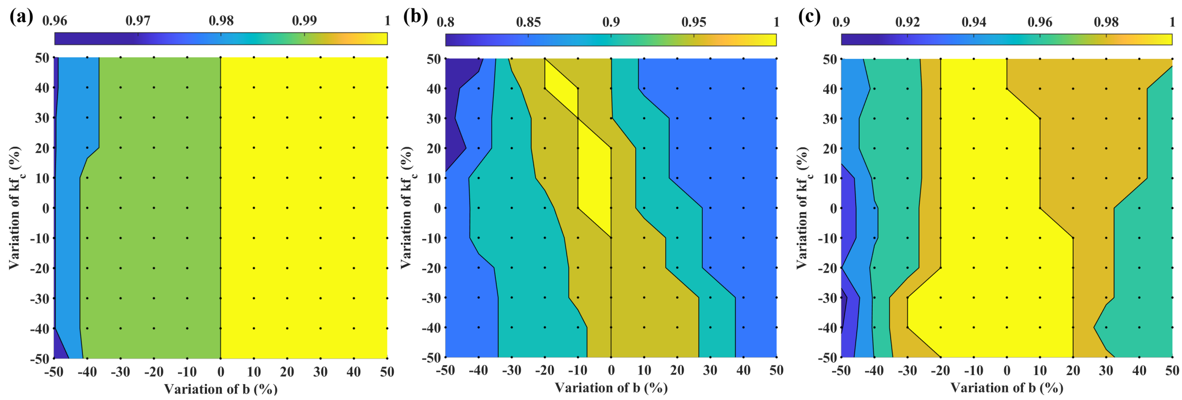

Figure 13: Robustness analysis results regarding the parameters b and kf_c for above-mentioned numerical examples: (a) railroad track, (b) welded joint and (c) adhesively composite joint; contour maps depict the F-measure of the clustering outcomes, and its amplitude indicated by the color bar annotations.

are recommended for regular waveguides; and b range [0.35, 0.65] and kf_c range [0,0.2] are preferred for relatively complex waveguide problems.

4.2. Effects of frequency discretization size

The selection of appropriate frequency discretization sizes is critical for tracing frequency-discrete eigen-solutions. The excessively coarse discretization size can lead to a reduction in the accuracy of mode tracing results, whilst choosing too fine frequency step will result in much higher computational expenses. Thus, a trade-off between the clustering accuracy and efficiency has to be achieved. Herein, analysis of the distribution of elements in the similarity matrix S can provide a measure for alarming the possible false clustering.

We take the numerical example of guided wave propagation in the prestressed plate as described in Section.3.5, and varied frequency discretization sizes ranging from 4kHz to 30kHz were utilized for the SAFE calculations. The corresponding distribution of elements S_{ij} in the similarity matrix is visualized in Fig.14, with the indication of their percentage across all similarities. The S0 and SH0 modes have been mistakenly identified in the process of AP clustering as the frequency discretization size is greater than 20kHz, and the F-measure associated with the cases of 20kHz and 30kHz has dropped to around 0.85. Upon closer examination of their S_{ij} distributions, the elements falling within the range $[-1, -0.9)$ take the percentage exceeding 3.7% in the similarity matrix, leading to false clustering. It can be predicted that a relatively high percentage of elements in the range of $[-1, -0.9)$ indicates possible errors in the tracing results, signaling the requirement of even finer frequency discretization size. Detecting and mitigating false clustering is essential for ensuring the accuracy and reliability of the tracing results via the proposed AP clustering.

5. Conclusion

An innovative automated physics-driven mode-tracing method has been proposed in this study to accurately determine dispersion curves for guided wave modes in elastic waveguides, irrespective of the computation of eigen-solutions. The associated feature extraction has been achieved by the enhanced cosine distance measurement between frequency-discrete eigen-solutions and the weighted summation over their physical characteristics encompassing particle displacement, power flow and angular momentum,

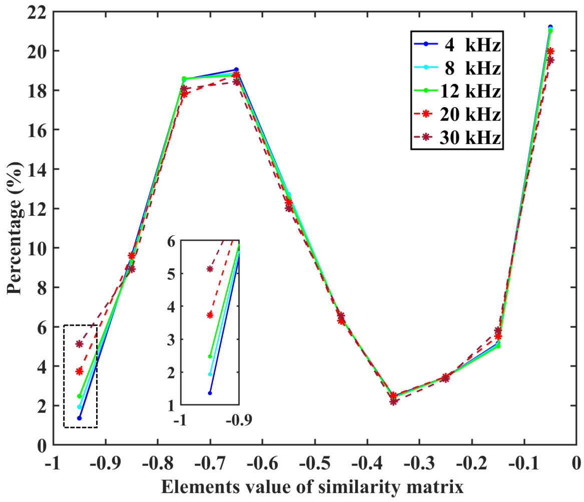

Figure 14: Distribution of elements in the similarity matrix for numerical evaluations with different frequency discretization sizes; instances of false clustering are denoted by dashed lines with asterisks, while accurate clustering is represented by solid lines with dots.

and the resultant similarity matrix has been constructed through the similarity propagation technique. The optimized AP algorithm has been used to process the similarity matrix, iteratively achieving a high-quality set of exemplars and corresponding clusters of guided wave modes. The proposed mode-tracing method has been implemented and well validated using five typical guided wave problems of relevance to NDE/SHM interests, with known alternative tracing results. The robustness analysis has been performed to evaluated the performance of the AP clustering and to enhance its practical applicability. Elevated by its remarkable accuracy and robustness, the proposed technique will emerge as a valuable tool for researchers to precisely determine dispersion relations for complex guided wave systems, thus contributing to the progress of quantitative NDE and SHM applications. Furthermore, the inherent physics-driven nature of this methodology implies its potential applicability to guided waves in diverse fields, such as seismology, electromagnetics, and optics and photonics, where dispersive phenomena are commonly encountered.

6. Acknowledgment

This work was supported by the National Natural Science Foundation of China [grant number 12004026,12374429,12134002] and the Young Elite Scientist Sponsorship Program by China Association for Science and Technology [grant number 2020QNRC002].

References

[1] P. Cawley, M. J. S. Lowe, D. N. Alleyne, B. Pavlakovic, P. Wilcox, Practical long range guided wave testing: application to pipes and rail, Mater. Eval. 61 (1) (2003) 66–74.

[2] J. L. Rose, M. J. Avioli, W. J. Song, Application and potential of guided wave rail inspection, Insight 44 (6) (2002) 353–358.

[3] Z. Su, L. Ye, Y. Lu, Guided Lamb waves for identification of damage in composite structures: A review, J. Sound Vibr. 295 (3) (2006) 753–780.

[4] T. Hayashi, M. Murase, Defect imaging with guided waves in a pipe, J. Acoust. Soc. Am. 117 (4) (2005) 2134–2140.

[5] A. J. Croxford, P. D. Wilcox, B. W. Drinkwater, G. Konstantinidis, Strategies for guided-wave structural health monitoring, Proc. R. Soc. A 463 (2007) 2961–2981.

[6] W. Ostachowicz, P. Kudela, M. Krawczuk, A. Zak, Guided waves in structures for SHM: the time-domain spectral element method, John Wiley & Sons, 2012.

[7] M. Castaings, B. Hosten, Ultrasonic guided waves for health monitoring of high-pressure composite tanks, NDT & E Int. 41 (8) (2008) 648–655.

[8] H. Matt, I. Bartoli, F. L. di Scalea, Ultrasonic guided wave monitoring of composite wing skin-to-spar bonded joints in aerospace structures, J. Acoust. Soc. Am. 118 (4) (2005) 2240–2252.

[9] D. E. Chimenti, Guided waves in plates and their use in materials characterization, Appl. Mech. Rev. 50 (5) (1997) 247–284.

[10] F. Simonetti, P. Cawley, A guided wave technique for the characterisation of highly attenuative viscoelastic materials, J. Acoust. Soc. Am. 114 (1) (2003) 158–165.

[11] B. Le Crom, M. Castaings, Shear horizontal guided wave modes to infer the shear stiffness of adhesive bond layers, J. Acoust. Soc. Am. 127 (4) (2010) 2220–2230.

[12] M. Deng, J. Yang, Characterization of elastic anisotropy of a solid plate using nonlinear lamb wave approach, J. Sound Vibr. 308 (1-2) (2007) 201–211.

[13] H. Cho, M. Hasanian, S. Shan, C. J. Lissenden, Nonlinear guided wave technique for localized damage detection in plates with surface-bonded sensors to receive lamb waves generated by shear-horizontal wave mixing, NDT E Int. 102 (2019) 35–46.

[14] P. B. Nagy, A. H. Nayfeh, Viscosity-induced attenuation of longitudinal guided waves in fluid-loaded rods, J. Acoust. Soc. Am. 100 (3) (1996) 1501–1508.

[15] P. Huthwaite, F. Simonetti, High-resolution guided wave tomography, Wave Motion 50 (5) (2013) 979–993.

[16] M. Mazzotti, A. Marzani, I. Bartoli, E. Viola, Guided waves dispersion analysis for prestressed viscoelastic waveguides by means of the SAFE method, Int. J. Solids Struct. 49 (18) (2012) 2359–2372.

[17] P. Wilcox, M. Lowe, P. Cawley, The effect of dispersion on long-range inspection using ultrasonic guided waves, NDT & E Int. 34 (1) (2001) 1–9.

[18] B. Drinkwater, M. Castaings, B. Hosten, The measurement of A_0 and S_0 Lamb wave attenuation to determine the normal and shear stiffnesses of a compressively loaded interface, J. Acoust. Soc. Am. 113 (6) (2003) 3161–3170.

[19] M. J. S. Lowe, Matrix techniques for modelling ultrasonic waves in multilayered media, IEEE Trans. Ultrason. Ferroelect. Freq. Contr. 42 (1995) 525–542.

[20] I. Bartoli, A. Marzani, F. L. di Scalea, E. Viola, Modeling wave propagation in damped waveguides of arbitrary cross-section, J. Sound Vibr. 295 (2006) 685–707.

[21] M. Castaings, M. J. S. Lowe, Finite element model for waves guided along solid systems of arbitrary section coupled to infinite solid media, J. Acoust. Soc. Am. 123 (2) (2008) 696–708.

[22] K. L. Nguyen, F. Treyssède, C. Hazard, Numerical modeling of three-dimensional open elastic waveguides combining semi-analytical finite element and perfectly matched layer methods, J. Sound Vibr. 344 (2015) 158–178.

[23] H. Gravenkamp, C. Song, J. Prager, A numerical approach for the computation of dispersion relations for plate structures using the Scaled Boundary Finite Element Method, J. Sound Vibr. 331 (11) (2012) 2543–2557.

[24] B. Mace, D. Duhamel, M. Brennan, L. Hinke, Wave number prediction using finite element analysis, in: N. l. Ivanov, M. J. Crocker (Eds.), 11th International Congress on Sound and Vibration, St. Petersburg, 2004, pp. 3241–3248.

[25] Ş. Sorohan, N. Constantin, M. Găvan, V. Anghel, Extraction of dispersion curves for waves propagating in free complex waveguides by standard finite element codes, Ultrasonics 51 (4) (2011) 503–515.

[26] C. Hakoda, J. Rose, P. Shokouhi, C. Lissenden, Using Floquet periodicity to easily calculate dispersion curves and wave structures of homogeneous waveguides, in: D. E. Chimenti, L. J. Bond (Eds.), Review of Progress in Quantitative NDE, Vol. 1949, AIP Publishing LLC, 2018, p. 020016.

[27] F. Simonetti, M. Lowe, On the meaning of lamb mode nonpropagating branches, J. Acoust. Soc. Am. 118 (1) (2005) 186–192.

[28] B. R. MacE, E. Manconi, Wave motion and dispersion phenomena: Veering, locking and strong coupling effects, J. Acoust. Soc. Am. 131 (2) (2012) 1015–1028.

[29] L. Houillon, M. Ichchou, L. Jezequel, Wave motion in thin-walled structures, J. Sound Vibr. 281 (3) (2005) 483–507.

[30] B. N. Pavlakovic, M. J. S. Lowe, D. N. Alleyne, P. Cawley, Disperse: A general purpose program for creating dispersion curves, in: D. O. Thompson, D. E. Chimenti (Eds.), Review of Progress in Quantitative NDE, Vol. 16, Plenum Press, New York, 1997, pp. 185–192.

[31] F. Krome, H. Gravenkamp, Analyzing modal behavior of guided waves using high order eigenvalue derivatives, Ultrasonics 71 (2016) 75–85.

[32] B. Zhu, L. Nechak, O. Bareille, Kriging metamodeling approach for predicting the dispersion curves for wave propagating in complex waveguide, J. Sound Vibr. 551 (2023).

[33] C. Morales, Comments on the MAC and the NCO, and a linear modal correlation coefficient, J. Sound Vibr. 282 (1-2) (2005) 529–537.

[34] M. V. Predoi, M. Castaings, B. Hosten, C. Bacon, Wave propagation along transversely periodic structures, J. Acoust. Soc. Am. 121 (4) (2007) 1935–1944.

[35] COMSOL, COMSOL Multiphysics Reference Manual, Version 5.6a by COMSOL MULTIPHYSICS, http://www.comsol.com/, 2020.

[36] B. A. Auld, Acoustic Fields and Waves in Solids, Vol. 1, Krieger Publishing Company, Malabar, Florida, 1990.

[37] R. Liu, H. Wang, X. Yu, Shared-nearest-neighbor-based clustering by fast search and find of density peaks, Information Sciences 450 (2018) 200–226.

[38] B. J. Frey, D. Dueck, Clustering by passing messages between data points, Science 315 (5814) (2007) 972–976.

[39] M. Castaings, B. Hosten, T. Kundu, Inversion of ultrasonic, plane-wave transmission data in composite plates to infer viscoelastic material properties, NDT & E Int. 33 (2000) 377–392.

[40] P. Wilcox, M. Evans, B. Pavlakovic, D. Alleyne, K. Vine, P. Cawley, M. Lowe, Guided wave testing of rail, Insight-Non-Destructive Testing and Condition Monitoring 45 (6) (2003) 413–420.

[41] X. Yu, P. Zuo, J. Xiao, Z. Fan, Detection of damage in welded joints using high order feature guided ultrasonic waves, Mech. Syst. Signal Process. 126 (2019) 176–192.

[42] Z. Fan, M. Castaings, M. J. Lowe, C. Biateau, P. Fromme, Feature-guided waves for monitoring adhesive shear modulus in bonded stiffeners, NDT & E Int. 54 (2013) 96–102.

[43] X. Yu, M. Ratassepp, Z. Fan, Damage detection in quasi-isotropic composite bends using ultrasonic feature guided waves, Compos. Sci. Technol. 141 (2017) 120–129.

[44] X. Yu, R. Qin, M. Deng, New insights into topographically feature guided waves (fgw) propagation in non-uniform elastic waveguides, Wave Motion 109 (2022) 102866.

[45] X. Yu, Z. Fan, M. Castaings, C. Biateau, Feature guided wave inspection of bond line defects between a stiffener and a composite plate, NDT & E Int. 89 (2017) 44–55.

[46] N. Gandhi, J. E. Michaels, S. J. Lee, Acoustoelastic Lamb wave propagation in biaxially stressed plates, J. Acoust. Soc. Am. 132 (3) (2012) 1284–1293.

[47] P. Zuo, X. Yu, Z. Fan, Acoustoelastic guided waves in waveguides with arbitrary prestress, J. Sound Vibr. 469 (2020) 115113.

[48] M. Halkidi, Y. Batistakis, M. Vazirgiannis, On clustering validation techniques, J. Intell. Inf. Syst. 17 (2) (2001) 107–145.

[49] C. D. Manning, P. Raghavan, H. Schütze, An Introduction to Information Retrieval, Vol. 8, Cambridge University Press, England, 2009.

[50] J. Wang, P. Neskovic, L. N. Cooper, Neighborhood size selection in the k-nearest-neighbor rule using statistical confidence, Pattern Recogn. 39 (3) (2006) 417–423.